Low intrinsic c-axis thermal conductivity in PVD grown epitaxial Sb_2Te_3 films

F. Rieger,[1] K. Kaiser,[2] G. Bendt,[2] V. Roddatis,[1] P. Thiessen,[1] S. Schulz,[2] and C. Jooss[1]
[1]*Institute of Material Physics, University of Göttingen, 37077 Göttingen, Germany*
[2]*Institute of Inorganic Chemistry and Center for Nanointegration Duisburg-Essen (Cenide), University of Duisburg-Essen, 45141 Essen, Germany*

(Received 9 February 2018; accepted 11 April 2018; published online 7 May 2018)

Accurate determination and comprehensive understanding of the intrinsic c-axis thermal conductivity κ_c of thermoelectric layered Sb_2Te_3 is of high importance for the development of strategies to optimize the figure of merit in thin film devices via heterostructures and defect engineering. We present here high precision measurements of κ_c of epitaxial Sb_2Te_3 thin films on Al_2O_3 substrates grown by physical vapor deposition in the temperature range of 100 K to 300 K. The Kapitza resistances of the involved interfaces have been determined and subtracted from the film data, allowing access to the intrinsic thermal conductivity of single crystalline Sb_2Te_3. At room temperature, we obtain $\kappa_c = 1.9$ W/m K, being much smaller than the in-plane thermal conductivity of $\kappa_{ab} = 5$ W/m K and even lower than the thermal conductivity of nano crystalline films of $\kappa_{nc} \approx 2.0$–2.6 W/m K published by Park *et al.* [Nanoscale Res. Lett. **9**, 96 (2014)]. High crystallinity and very low defect concentration of the films were confirmed by x-ray diffraction and high resolution transmission electron microscopy. Our data reveal that the phonon mean free path $l_{mfp}(T)$ is not limited by defect scattering and is of intrinsic nature, i.e., due to phonon-phonon scattering similar to other soft van der Waals type bonded layered systems. https://doi.org/10.1063/1.5025491

I. INTRODUCTION

Tetradymite-type materials such as Sb_2Te_3 and Bi_2Te_3 are thermoelectric materials with promising high figure of merit ZT close to 1 in a temperature range of 300–400 K which is promising for technical applications.[2] The thermoelectric efficiency of a material is given by the dimensionless figure of merit $ZT = (S^2\sigma/\kappa)T$ [S = Seebeck coefficient, σ = specific electrical conductivity, κ = thermal conductivity = sum of electronic κ_{el} and lattice κ_{la} contributions, T = absolute temperature (K)].[3] In order to achieve a high ZT, high Seebeck coefficients (S), high electrical conductivity (σ) and low thermal conductivity (κ) are required. For many thermoelectric relevant materials the lowering of lattice thermal conductivity by the introduction of grain boundaries or interfaces in heterostructures have been demonstrated.[4] Reduction of thermal conductivity down to $\kappa = 0.22$ W/m K by a factor of 7–8 was reported for Sb_2Te_3/Bi_2Te_3 multilayer structures by Venkatasubramanian *et al.*[5] The same author claimed a high ZT value of 2.4 for p-type Sb_2Te_3/Bi_2Te_3 multilayer structures.[6] This result could not be reproduced by other research groups and was later questioned since the superlattices have been shown to be unstable at elevated temperatures.[7–9] Here, reduced cross-plane thermal conductivity (0.55 to 0.6 W/m K) is due to nanoalloying of the superlattice at elevated temperatures was observed, while no measurable reduction of the thermal conductivity by the superlattice-type 2D nanostructuring was found (see also the overview in Ref. 8) therefore pointing against simultaneous low thermal and high electrical cross plane conductivities in such systems.

High-quality Sb_2Te_3 films have been grown by use of different methods, including molecular beam epitaxy (MBE),[10–12] RF-magnetron sputtering,[13] pulsed laser deposition (PLD),[14,15] metal organic chemical vapor deposition (MOCVD)[16,17] and thermal (co-)evaporation,[18–21] respectively.[22,23] Among these, thermal (co-) evaporation is of particular interest, since it allows the deposition of highly stoichiometric, impurity-free Sb_2Te_3 thin films on rather large substrates with high growth rates starting with commercially available, high-purity Sb_2Te_3 powder. As a consequence, it is a far less expensive and less time-consuming method compared to MOCVD, MBE and sputtering, but to the best of our knowledge, its capability for the epitaxial growth of highly c-oriented Sb_2Te_3 films has not been demonstrated.

For an understanding of the thermal conductivity in superlattices or nanocrystalline materials, reliable data of the anisotropic intrinsic thermal conductivity of single crystalline tellurides is required. Whereas temperature dependent data for the in-plane thermal conductivity κ_{ab} in Sb_2Te_3 single crystals is published,[24,25] to the best of our knowledge, data on c-axis thermal conductivity κ_c is only reported for room temperature.[26] Park *et al.*[1] measured the thermal conductivity of magnetron-sputtered nanocrystalline Sb_2Te_3 films, where the grain size has been varied by annealing. Remarkably, the room temperature's thermal conductivity $\kappa_{ab} = 5$ W/m K, $\kappa_c = 1.9$ W/m K shows a pronounced anisotropy $A = \kappa_{ab}/\kappa_c \approx 2.6$. Consequently, the thermal conductivity in nanocrystalline films in the range of $\kappa_{nc} \approx 2.0$–2.6 W/m K is certainly strongly influenced by the anisotropy. Temperature dependent $\kappa_c(T)$ measurements are thus highly desirable for the understanding of nanostructured tellurides and for basic insights into the transport mechanism of phonons across layered systems which are connected only via

van der Waals bonding. Furthermore, for the application in thermoelectric devices the c-axis component $\kappa_c(T)$ is the most relevant.

Here, we present $\kappa_c(T)$ in the range between $T = 100–300\,K$ determined by the 3ω method. Highly crystalline epitaxial Sb_2Te_3 films with a very low defect concentration have been grown by physical vapor deposition (PVD). The epitaxial growth and crystallinity is confirmed by x-ray diffractometry as well as by transmission electron microscopy (TEM). High resolution transmission electron microscopy (HRTEM) shows a low density of stacking faults and grain boundaries. In order to determine the intrinsic $\kappa_c(T)$, a careful determination and subtraction of the Kapitza resistances of all involved interfaces between the Sb_2Te_3 films and the substrate as well as the 3ω heater structure is required. This is carried out by variation of the thickness of the Sb_2Te_3 films as well as of the SiO_2 layer, required for electrical insulation of the Pt heater structures from the thermoelectric films in the 3ω measurements. The paper is organized as follows: In Sec. II, we present the growth and characterization of the PVD Sb_2Te_3 films as well as the introduction of the used 3ω setup. We continue in presenting the thermal conductivity measurements and the HRTEM characterization. In Sec. IV, the obtained intrinsic $\kappa_c(T)$ of the epitaxial films is compared with the literature data of single crystalline and nanocrystalline Sb_2Te_3 samples, and the determined phonon mean free path is discussed in the light of the determined crystal- and microstructure. This allows for conclusions on the intrinsic limitation of the c-axis phonon thermal conductivity in the van der Waals type layered system.

II. EXPERIMENTAL

A. Film preparation via PVD

Epitaxial thin films of Sb_2Te_3 were grown on $10 \times 10\,mm$ *c*-orientated sapphire [Al_2O_3 (0001)] substrates in a vertical PVD-reactor at a substrate temperature of 330 °C. Commercial Sb_2Te_3 powder (150 mg, 99.999% abcr) was evaporated at 570 °C at 20 mbar within 15 minutes.

According to XPS studies (Fig. S1), the Sb_2Te_3 films show a thin (1–3 nm) oxide surface layer due to post-oxidation processes during transport and handling of the films under atmosphere. However, the thickness of the oxide layer did not increase with time as it was shown by analyzing a sample that was stored for 1 month under ambient conditions.

A Bruker D8 Advance powder diffractometer in a Bragg-Brentano geometry with Cu-Kα radiation ($\lambda = 1.5418$ Å) was used for XRD studies. A typical XRD pattern as displayed in Fig. 1 shows the characteristic 00*l* ($l = 3, 6, 9, 12, \ldots$) reflections for *c*-orientated antimony telluride (PDF: 71-393). No other crystalline phases are present.

SEM investigations done at a *FEI Nova NanoSEM 650* shown in Fig. 2 reveal a flat surface morphology. All films show island growth mode. Crystallites of some μm size are observed which are all c-oriented as confirmed by XRD and TEM. Flatness is an important requirement for depositing a proper insulation layer and Pt heater structures for reliable 3ω measurements.

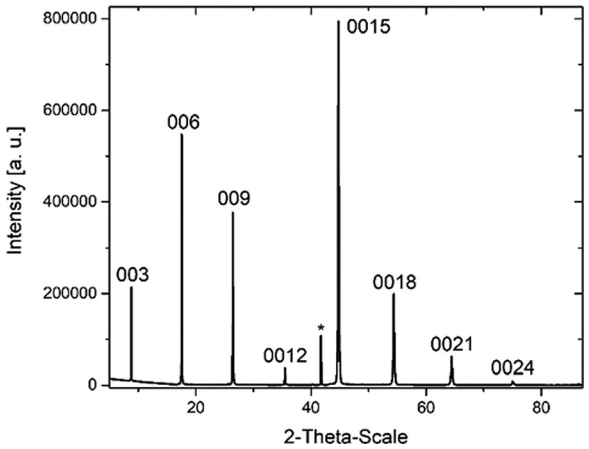

FIG. 1. X-ray diffractogram of a PVD grown Sb_2Te_3 film on a *c*-oriented Al_2O_3 substrate. The asterisk corresponds to the 006 reflection of the Al_2O_3 substrate.

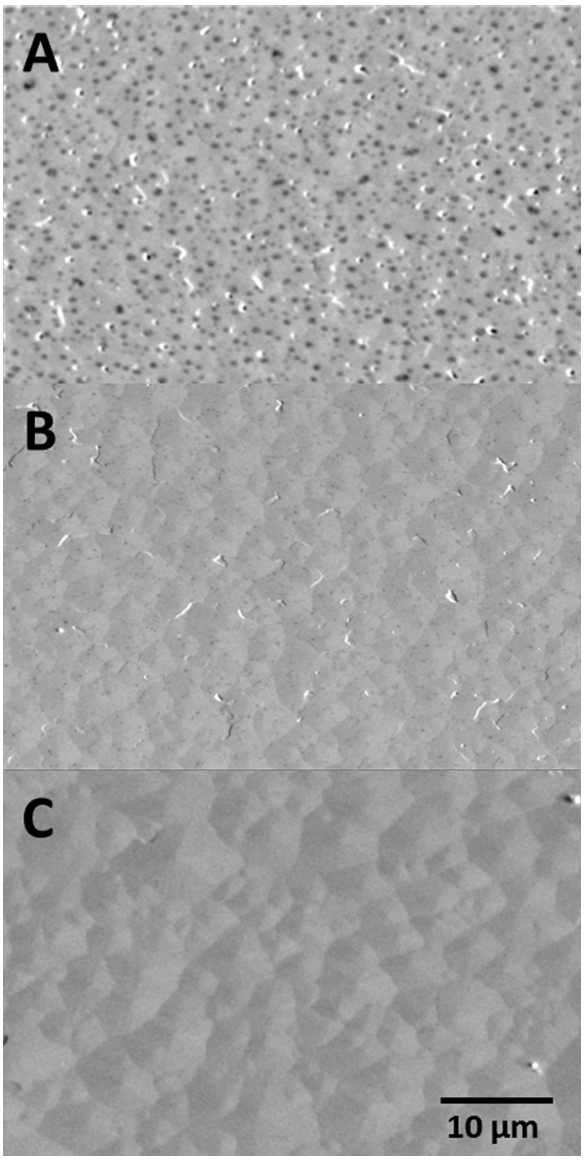

FIG. 2. SEM images of Sb_2Te_3 samples with different thicknesses taken under 45° inclination, (a) 191, (b) 487, and (c) 1184 nm. The dark contrast in Fig. 2(a) for the thinnest film is most probable due to pinholes.

B. High resolution TEM

TEM lamellas have been prepared via Focused Ion Beam (FIB) technology using a *Nova NanoLab 600* (FEI, Netherlands), operated at 30 kV and 5 kV, and partially followed by a cleaning argon ion milling step in a Gatan PIPS. HRTEM, STEM and EELS studies have been performed at a C_S corrected FEI Titan 80–300 kV operated at 300 kV.

C. Sample geometry for thermal conductivity measurements

The geometry of the samples including the Pt heater structures for the 3ω measurement is shown in Fig. 3. Subsequently, the SiO_2 insulating layer and the 200 nm thick Pt layer have been deposited by ion beam deposition in a negative resist mask that has been fabricated by electron beam lithography. After deposition of the films, the resist is removed by solving it in acetone followed by a lift-off process. To minimize possible electric short circuits between the heater and the film, the size of the heater area on top of the Sb_2Te_3 film is minimized. Consequently, the Sb_2Te_3 film covers only one corner of the substrate. This allows depositing three heater structures, one on the substrate and two close to the film, where only the relevant transport strip is on top of the thermoelectric film, respectively. This geometry has been chosen for verification. The heater on top of the SiO_2/substrate is used for measuring the thermal conductivity of the SiO_2 insulating layer.

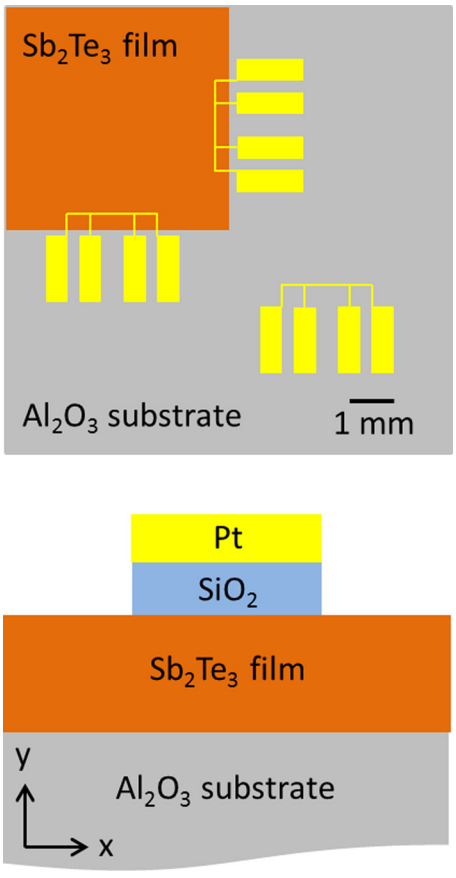

FIG. 3. Top view and cross section of the sample geometry and the used heater structure for the 3ω measurement. The coordinate system is used in the formula shown below.

The thicknesses of the film, the SiO_2 layer and the Pt heater are measured by profilometry, X-ray reflectometry and TEM. The heater width $2b$ has been measured via SEM for every individual heater structure. Due to highly reproducible lithography procedures, the variations are with $2b = 10.55 \pm 0.1\,\mu$m very small. The total heater length is 2 mm; the segment between the voltage sense connections has a length of 1 mm. The TEM characterization of the SiO_2/Pt stack (Fig. S2 in the supplementary material) shows a very flat SiO_2 film with complete surface coverage. Selection of the minimum SiO_2 thickness of 60 nm was made based on exclusion of electric shortcuts. Samples have been electrically contacted by silver paste and soldering.

D. Thermal conductivity measurements by the 3ω method

Cross plane thermal conductivity measurements of the films have been performed by the 3ω-technique in the temperature range of 40 to 310 K in high vacuum. The temperature was controlled by using an electric heater and simultaneously a closed cycle helium cryostat. Used frequencies for the AC current through the heater structure were in the range of 210 to 1010 Hz. The 3ω set up in Göttingen is based on a description of Raudzis[27] and further optimized with respect to reference resistances and software control. An *eLockIn 204/2* (Anfatec, Germany) is used to extract the $U_{3\omega}$ signal.

We analyze the data based on an extension of the method of Cahill,[28] taking into account the anisotropy of film, the heat spread in the film as well as the heat transfer conditions at the backside of the substrate as suggested by Borca-Tasciuc *et al.*[29] We found approximately adiabatic boundary conditions at the substrates backside thermal contact. In the following, the indexes "s" and "f" are used for substrate and the film, respectively. We fit the $\Delta T(\ln(\omega))$ data to the frequency dependent integral function

$$|\Delta T| = \left| \frac{P}{l\pi\kappa_{s,y}} \times \int_0^\infty \frac{\sin^2(kb)}{\tanh\left(t_s\sqrt{\eta_s k^2+q^2}\right)(kb)^2\sqrt{\eta_s k^2+q^2}}dk + \Delta T_{tot} \right|, \tag{1a}$$

$$\kappa_{f,y} = \sqrt{\frac{1}{4}\Xi^2 + \frac{\eta_s}{\eta_f}\cdot\kappa_{s,y}^2} - \frac{1}{2}\Xi, \tag{1b}$$

$$\Xi = \frac{\eta_s}{\eta_f}\cdot\frac{2bl}{t_f P}\cdot\Delta T_f\cdot\kappa_{s,y}^2, \tag{1c}$$

where $\kappa_{s,y}$ and $\kappa_{f,y}$ are the cross plane components of the thermal conductivities, ΔT is the total thermal offset in the heater, ΔT_{tot} is the out of plane component of the offset created by the film, insulation layer and Kapitza resistances, ΔT_f is the offset created by the film only, P/l is the applied power per length of the heater, $2b$ is the width of the heater, t_s and t_f are the thicknesses. Furthermore, q is the inverse of the thermal penetration depth of the substrate, which depends on the temperature and frequency. The fitting parameters are

$\kappa_{s,y}$ and ΔT_f. Using the absolute value of the $\Delta T(\omega)$ oscillation, one can avoid the measurement of phase shifts. This is often a critical source of errors in 3ω measurements. Equations (1b) and (1c) are derived from Tong and Majumdar[30] as shown in the supplement. Equation (1b) includes a correction for horizontal heat transfer through the film. It is used for more accurate results, even though here it only has a very small impact due to high substrate and low film thermal conductivities. We use anisotropy ratios for substrate and film of $\eta_s = 0.93$ and $\eta_f = 2.3$, respectively. The changes in the determined c-axis thermal conductivity of the films in comparison to the isotropic limit $\eta_s = \eta_f = 1$ are however within error bars.

The shown error bars are calculated by error propagation from Eq. (1), using the experimental errors in the heater's width and length, film thickness and the standard deviation of the two fit parameters ΔT_{tot} and $\kappa_{s,y}$ in Eq. (1a).

In order to determine the intrinsic thermal conductivity of the thermoelectric Sb_2Te_3 films, the subtraction of the thermal conductivity of the SiO_2 insulation layer and the Kapitza resistances is necessary. For that reason, a SiO_2 layer thickness series for the Kapitza resistances in the reference samples has been prepared and measured containing 9 samples from 10 to 200 nm SiO_2 thicknesses. Furthermore, 7 samples of Sb_2Te_3 with thicknesses between 191 and 1184 nm were prepared and measured, in order to determine the Kapitza resistances of the two interfaces involving the Sb_2Te_3 film (see Fig. 4).

III. RESULTS

A. Determination of the Kapitza resistances

The Kapitza resistance of a pair of interfaces of a thin film can be determined by studying the ΔT oscillation as a function of the film thickness d and extrapolating to $\Delta T(d \rightarrow 0)$. In our stack of thin films, two different Kapitza resistances have to be considered: (i) The Kapitza resistance of the two interfaces connected to the SiO_2 insulation layer (SiO_2-Sb_2Te_3 and SiO_2-Pt) which were named Kapitza A in the following. (ii) The Kapitza resistance of the two interfaces connected to the Sb_2Te_3 film (Al_2O_3-Sb_2Te_3 and Sb_2Te_3-SiO_2) plus the SiO_2-Pt interface at the Pt heater, were named Kapitza B, in the following.

In order to determine Kapitza A, ΔT was measured as a function of the SiO_2 layer thickness d_{SiO2} (supplementary material, Fig. S3). Below 60 nm SiO_2 thickness, a linear dependence of $\Delta T(t_{SiO2})$ was observed which turned a non-linear increase at the higher SiO_2 thickness most probably due to the thickness of the dependent microstructural changes. Both the linear fit between 10 nm to 60 nm as well the polynomial 2nd order fit between 10 nm and 200 nm gave similar results for $\Delta T(d_{SiO2} \rightarrow 0)$ (see supplementary material Fig. S4). The results for the linear fits as a function of temperature were shown in Fig. 5.

For determination of Kapitza B, ΔT was measured as a function of the Sb_2Te_3 layer thickness t_f, showing a linear dependence of $\Delta T(t_f)$ over the entire thickness range from $t_f = 191$ nm to 1184 nm. An exemplary fit was shown in the supplementary material Fig. S5. The resulting Kapitza B resistance as a function of temperature was shown in Fig. 5. The SiO_2 contribution wa subtracted. Below 100 K the thermal penetration depth in the Al_2O_3 substrate was too large for the used adiabatic boundary condition for the 3ω data evaluation. This was due to the strong rise in the thermal conductivity in Al_2O_3 at that temperature range, where thermal waves could have been reflected at the backside of the substrate. In the measured temperature range Kapitza B was constant. This might have been be due to the relatively low Debye temperature of Sb_2Te_3 of 157 K. Kapitza B was found to be much higher than Kapitza A. This was explained by three different properties: The Debye temperature in Al_2O_3 was 1047 K much above that of Sb_2Te_3 and thus there was a huge acoustic mismatch between Sb_2Te_3 and Al_2O_3 as expected. Additionally, the weak van der Waals bonding between substrate and film contributed to a huge thermal boundary resistance. Furthermore, Sb_2Te_3 showed an electronic contribution to the thermal conductivity while Al_2O_3 was an electric insulator.

B. Determination of the cross plane thermal conductivity of Sb_2Te_3

Since the Kapitza resistances significantly contributed to the total ΔT oscillation of the film stack, the thermal

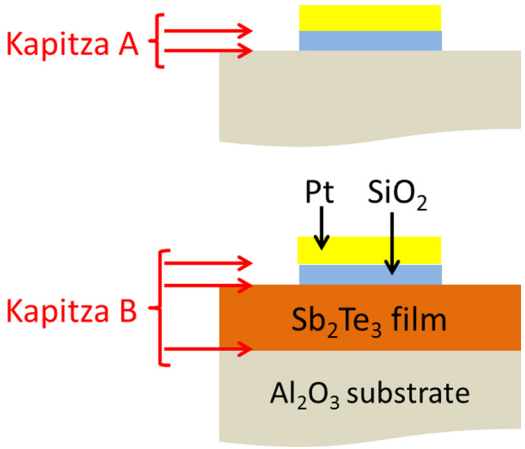

FIG. 4. Sketch of the cross sections of samples of the SiO_2 and the Sb_2Te_3 thickness series, showing the interfaces that are involved in the Kapitza resistances A and B.

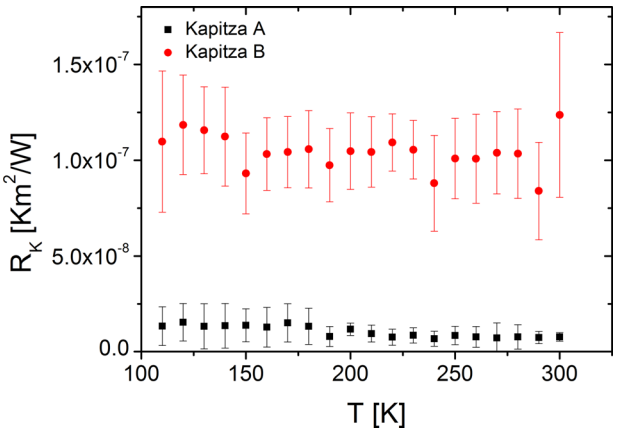

FIG. 5. The Kapitza resistances A and B as defined in Fig. 4 determined from a series of samples with different SiO_2 and Sb_2Te_3 layer thicknesses as described in the text.

conductivity of the Sb_2Te_3 film would have been underestimated. In the first step, the Kapitza A thermal offset was subtracted from the offset of the reference measurement of the SiO_2 insulation layer, in order to get the ΔT caused by the SiO_2 layer only. The resulting contribution of SiO_2 and Kapitza B was then subtracted from the thermal offset of the stack in order to obtain the intrinsic out of plane thermal conductivity of those Sb_2Te_3 films.

As a result, a precise determination of the intrinsic thermal conductivity as a function of temperature in the range between 100 K and 300 K was achieved. The influence of the Kapitza resistances were seen in Fig. 6. Obviously, the correction of the interface resistances was very important for the determination of the intrinsic κ_c(T) of Sb_2Te_3. The resulting measurement errors were lowfor small κ_c values due to the corresponding high thermal offset. On an average they were estimated to be below 15% which was quite reasonable for thermal thin film measurements.

C. HRTEM results

Some samples from the Sb_2Te_3 layer thickness series were investigated using HRTEM and HRSTEM to gain information about their atomic structure and density of defects. Exemplary images are shown for a 191 nm sample in Figs. 7(a) and 7(b). The study of the film-substrate interface using EELS showed that all samples start growing with one or two quintuple layers of partially oxidized Sb_2Te_{3-x} and were also visible in the enhanced disorder of one monolayer in the HRTEM images.

EELS results at three positions marked at Fig. 7(b) were shown in Fig. 7(c). They were based on the analysis of the energy range of 450 to 650 eV. We used the Sb M edge (528 eV), the O K edge (532 eV) and the Te M edge (572 eV) to obtain the relative concentrations by using Gaussian plots. An exponential background was subtracted from the original high energy loss spectra. The original data was shown in Fig. S6 (supplementary material). The background subtracted spectra together with the used Gaussian fits were seen in the supplementary material Figs. S7, S8, and S9. Since the energy edges of all three elements wereclose, the overlap of the maxima was the origin of possible errors. Nevertheless, the result fit very well to our expectations: Position 1 on the substrate showedonly O as it was located on the Al_2O_3 substrate while Position 3 was approximately 6 nm away from the substrate consisting of only Sb and Te in the expected ratio of 2:3. Position 2 at the first quintuple layer exhibited a slightly higher Sb to Te ratio and a small O content. We suggest that the formation of Sb was enriched $Sb_2Te_{3-x}O_y$ during the film growth by intermixing with surface oxygen from the substrate. This interfacial layer exhibited significant disorder visible in the high

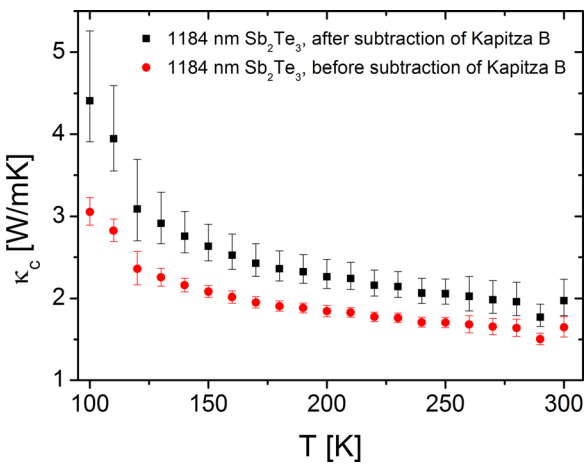

FIG. 6. Thermal conductivity of a representative Sb_2Te_3 film without (red) and with (black) subtraction of the Kapitza resistance B.

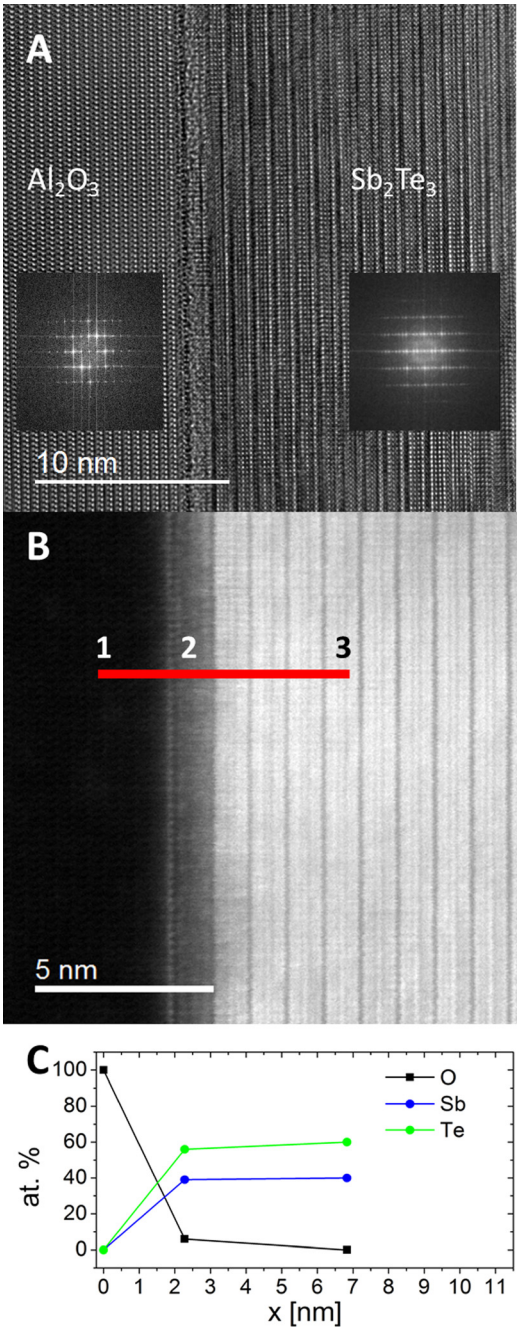

FIG. 7. Interface Al_2O_3-Sb_2Te_3 (191 nm thick). (a) HRTEM image and, FFTs show epitaxial c-axis oriented film. (b) STEM image of the interface, (c) EELS results for O K edge, Sb M edge and Te M edge at three different positions marked in B.

resolution images, however its presence did not affect the epitaxial growth of the Sb_2Te_3.

A very low defect concentration was observed in all the samples. The concentration of the stacking faults was increasing slowly starting at approximately 150 nm thickness with the increasing distance to the substrate. Moreover, the 1184 nm thick Sb_2Te_3 film showed the formation of differently oriented surface grains. They should have been formed due to a reduced growth in temperature at the increasing film thickness, due to the thermal gradient between the substrate and the top area of the film (Fig. 8).

IV. DISCUSSION

After careful subtraction of the extrinsic contributions of the interfaces and the insulation layers, the determined intrinsic out of the plane thermal conductivity $\kappa_c(T)$ of Sb_2Te_3 epitaxial films of different thicknesses are shown in Fig. 9(a). Deviations for $T < 140$ K was because of $q^{-1} \rightarrow t_s$ and thus the used adiabatic thermal boundary condition for the back contact of the substrate was getting increasingly inaccurate with decreasing T. C-axis conductivity of a representative film was compared to κ_c and $\kappa_{a,b}(T)$ data from literature in Fig. 9(b). We selected the thickest film because of the lowest error. In literature, only the c-axis thermal conductivity data for Sb_2Te_3 single crystals at room temperature has been found.[26] It was determined by measuring the thermal diffusivity via an open-cell photoacoustic method in the rear-side illumination configuration. The measurement was performed on Sb_2Te_3 single crystals prepared in sealed quartz ampullas at 850 °C. To the best of our knowledge, no temperature dependent $\kappa_c(T)$ values were available in the literature. The value $\kappa_c = 1.65 \pm 0.11$ W/m K given by Yáñez-Limón *et al.*[26] well agrees with our $\kappa_c(300\,\mathrm{K})$ data for epitaxial thin films. This confirms the low defect concentration and high crystallinity of our PVD grown c-oriented Sb_2Te_3 films as found by HRTEM analysis.

The in-plane thermal conductivity $\kappa_{ab}(T)$ was measured by a longitudinal steady-state technique at Sb_2Te_3 single crystals grown by a modified Bridgeman method.[24] The $\kappa_{ab}(T)$ is several times larger than the measured $\kappa_c(T)$ of our epitaxial films, indicating temperature dependent anisotropy $A(T)$ between 1.5 and 2.6 (ignoring the obviously deviating value of our measurement at 290 K).

Figure 9(b) also shows the thermal conductivity of nanocrystalline films prepared by RF-magnetron sputtering at a room temperature on Si measured by the 3ω method.[1] The films were annealed at different temperatures between 200 °C and 350 °C in order to modify the grain size between 88 nm and 129 nm. Without the effect of grain boundary scattering, the average thermal conductivity in nanocrystalline films would be given by $\kappa_{av} = \sqrt{\kappa_c \kappa_{ab}} = \kappa_c \sqrt{A} \approx (1.2\text{–}1.6)\ \kappa_c$. Indeed, as shown in Fig. 9(b), above T = 200 K, the thermal conductivity of the nanocrystalline films was close to the $\kappa_c(T)$ of our single crystalline films. Consequently, the effect

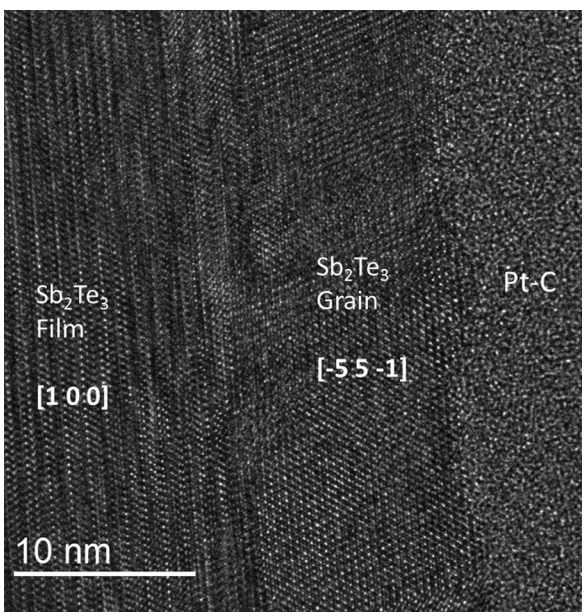

FIG. 8. Upper part of a 1184 nm thick Sb_2Te_3 film covered by the Pt-C protection layer. It shows a slightly higher defect concentration followed by thin grains with different orientation but same composition.

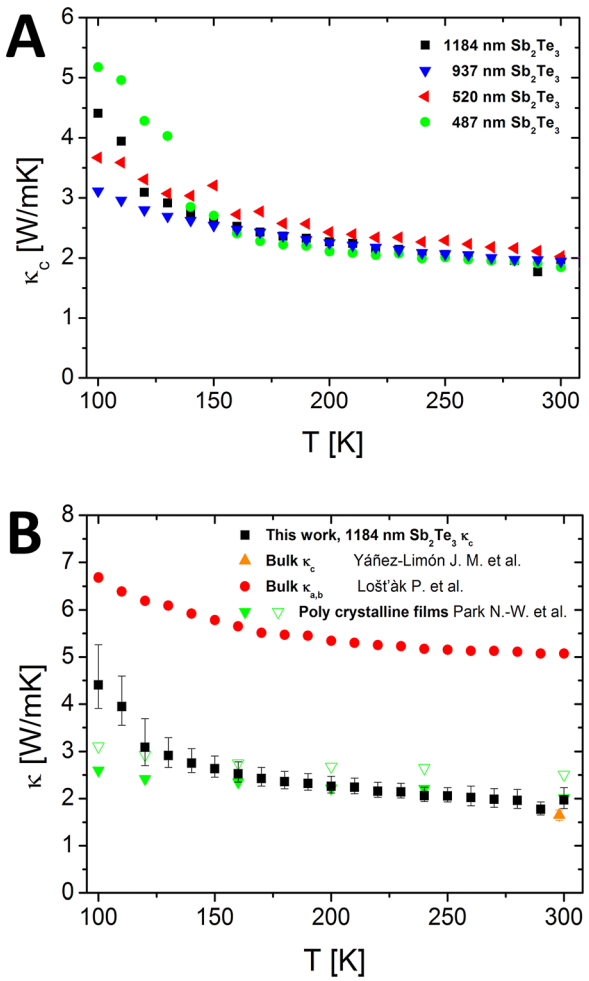

FIG. 9. (a) C-axis thermal conductivity κ_c of the PVD grown Sb_2Te_3 films of different thicknesses after correction for Kapitza resistances and the contribution of the SiO_2 insulation layer. (b) The result for $\kappa_c(T)$ for the 1184 nm thick film is compared with the room temperature value of κ_c and $\kappa_{a,b}(T)$ measured at single crystalline bulk Sb_2Te_3.[24,26] In addition, the thermal conductivity of nanocrystalline sputtered Sb_2Te_3 films with two different average grain sizes 88 nm (filled green triangles) 129 nm (empty green triangles) is presented for comparison.[1]

of grain boundary scattering at grain sizes of the order of 100 nm seemed to be quite low and was only visible at temperatures below 120 K.

Next, we applied a simple approximation of kinetic theory for the phonon thermal conductivity to correlate the estimated phonon mean free path l_{mfp} with the average defect density in our epitaxial films. In order to get an estimate of l_{mfp}, the electronic contribution to κ_c was subtracted, i.e.,

$$\kappa_{c,l}(T) = \kappa_c - \kappa_{c,e} \approx \frac{1}{3} C_V v l_{mfp}, \tag{2}$$

where $\kappa_{c,e}$ is the electron contribution, C_v is the specific heat and v is the average velocity of acoustic phonon modes. We took $\kappa_{c,e} = 1.03$ W/m K from Ref. 26. $C_v(T)$ from 4 up to 280 K that has been published by Dutta *et al.*[31] We determine $C_v(300\,\mathrm{K})$ by extrapolation that for Sb_2Te_3 the increase was very small in that temperature region. The sound velocity parallel to the c axis v_c was been obtained using the stiffness matrix C (Ref. 32) and the density ρ by using the following formula was adopted from Zheng *et al.*[33]

$$v_c = \frac{1}{3} v_L + \frac{2}{3} v_T = \frac{1}{3}\sqrt{\left(\frac{C_{33}}{\rho}\right)} + \frac{2}{3}\sqrt{\left(\frac{C_{44}}{\rho}\right)}. \tag{3}$$

Temperature dependent measurement of σ_c published by Lošťák *et al.*[25] revealed an almost constant $\kappa_{c,e}(T)$. We took a temperature independent absolute value of $\kappa_{c,e}$ from Ref. 26. The result for the phonon mean free path l_{mfp} parallel to the c-axis was shown in Fig. 10: The order of magnitude of l_{mfp} was in the range of only a few nm for all the temperatures and showed a monotonously decreasing temperature dependence.

The approximation of Eq. (2) for an estimate of the mean free path of a representative phonon from the lattice thermal conductivity was only valid in isotropic materials. For strongly anisotropic vdW materials such as graphite ($A = 300$), this equation has led to a strong underestimate of l_{mfp} in c-direction, because of a strong variation of the density of states in different directions.[34–36] This had the consequence that specific heat transported into the c-axis is reduced compared to the isotropic value $\frac{1}{3} C_V(T)$. In comparison to graphite, the thermal conductivity anisotropy of Sb_2Te_3 was however two orders of magnitude smaller. We thus suggested correcting to the specific heat transported in c-direction by the anisotropy ratio of the highest acoustic phonon frequency in the c- and ab-directions, respectively,

$$C_{V,mod} = C_V \frac{\omega_{ac,c}}{\omega_{ac,ab}}. \tag{4}$$

Using $\omega_{ac,c}/\omega_{ac,ab} \approx 0.62$ from Ref. 37, the estimate of l_{mfp} in c-direction was increased by around 60% as shown in Fig. 10.

In comparison, the observed density of the stacking faults in the 487 nm thick Sb_2Te_3 film was approx. $10^{10}/cm^2$, in the sample with 1184 nm thickness it was estimated to be around $2 \times 10^{10}/cm^2$. This translated into a mean distance between stacking faults parallel to the c-axis of about 50 to 100 nm and was much larger than the estimated phonon mean free path. Although the density of the point defects could not be directly measured, we argued that their impact on l_{mfp} in PVD grown films was negligible. Since the growth of PVD films proceeded near to the thermal equilibrium, the point defect concentration should be close to the thermal equilibrium concentration. For example, the defect of lowest formation energy ΔE in Sb_2Te_3 is the antisite defect with $\Delta E = 0.35$ eV and a measured room temperature concentration of $8–10 \times 10^{19}\,cm^{-3}$ (see Ref. 38). This was translated in an anti-site defect in 1 out of 26 unit cells and thus an average distance in c-direction of 81.4 nm.

Noted that l_{mfp} in c-direction derived from the kinetic theory may represent the lower bound values, even after correction for anisotropy. Taking the phonon dispersion into account typically yielded a higher l_{mfp} as e.g., shown for silicon.[39] In addition, a recent study[40] has shown that for a vdW material ($Ta_2Pd_3Se_8$) of less degree of anisotropy than graphite, the l_{mfp} along the vdW interaction direction could be tens of nanometers long. Our conclusion about the intrinsic origin of the low $\kappa_c(T)$ in our Sb_2Te_3 films thus depends on the assumption that phonon dispersion affects l_{mfp} as obtained by kinetic theory by less than one order of magnitude.

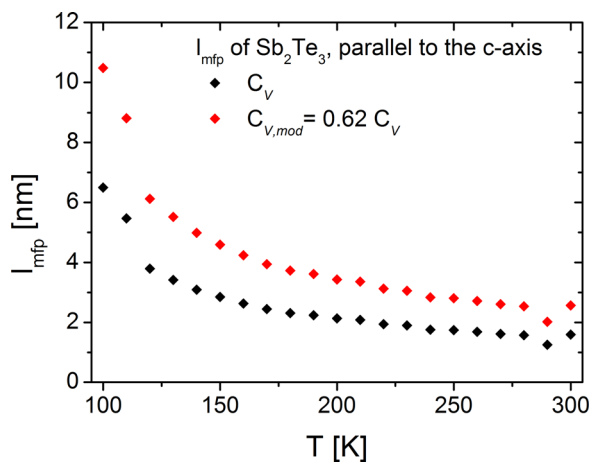

FIG. 10. Phonon mean free path of Sb_2Te_3 parallel to the c-axis, based on κ_c calculated as described in the text.

V. SUMMARY AND CONCLUSION

We have carried out careful measurements of the c-axis thermal conductivity in high quality nearly single crystalline epitaxial Sb_2Te_3 thin films using the 3ω method. In order to determine the intrinsic κ_c(T), the contribution of the Kapitza resistances and the thermal resistance of the electrical insulation layer were measured. The obtained Kapitza resistance of the two interfaces between the layered Sb_2Te_3 film sandwiched by Al_2O_3 and SiO_2 was with $R_K \geq 10^{-7}\,Km^2/W$ which is relatively large. However, the value fits well to the range of values of interfaces with large acoustic impedance mismatch.[41] Our result on the intrinsic c-axis thermal conductivity of epitaxial thin films indeed confirms the low $\kappa_c(300\,K)$ value of an Sb_2Te_3 single crystal in Ref. 26. After taking into account the electronic contribution to κ_c(T), we approximately calculated the temperature dependent phonon mean free path. We argue that the intrinsic phonon mean

free path due to phonon-phonon scattering is dominating κ_c(T) above the Debye temperature [$\theta_D = 157$ K (Ref. 42)]. Although we cannot entirely rule out the effect of point defects on l_{mfp}, their effect at thermal equilibrium concentration is small. Consequently, we obtain a low intrinsic $\kappa_c(T)$ in epitaxial highly crystalline Sb_2Te_3 films grown by PVD close to thermal equilibrium.

We observe a weak decrease in κ_c(T) with increasing temperature. Such a temperature characteristic is typically observed for the c-direction in van der Waals bound layered systems with relatively low Debye temperature such as WSe_2 at low defect density[43] or $Ca_3Co_4O_9$[44] due to phonon-phonon scattering. The low intrinsic $\kappa_c(T)$ as well as the temperature characteristics in Sb_2Te_3 support the idea of a generally low $\kappa_c(T)$ for layered materials with van der Waals bonding. Furthermore, we conclude that the reduced thermal conductivity of nanocrystalline films in Ref. 1 compared to κ_{ab} is mostly due to the low c-axis contribution, suggesting that an effective pathway for the reduction of the thermal conductivity in c-axis oriented films is predominantly enhancing point defect scattering by alloying of pure systems or by interdiffusion of different chemical species in superlattices.

SUPPLEMENTARY MATERIAL

See supplementary material document for the derivation of Eqs. (1b) and (1c) from literature and figures named S1 to S9.

ACKNOWLEDGMENTS

Financial support by the Deutsche Forschungsgemeinschaft DFG (S. Schulz, Project SCHU 1069/20-1; C. Jooss, Project JO 348/12-1) is gratefully acknowledged.

[1]N.-W. Park, W.-Y. Lee, J.-A. Kim, K. Song, H. Lim, W.-D. Kim, S.-G. Yoon, and S.-K. Lee, Nanoscale Res. Lett. **9**, 96 (2014).
[2]T. M. Trittet and M. A. Subramanian, MRS Bull. **31**, 188 (2006).
[3]D. M. Rowe, *Handbook of Thermoelectrics* (CRC Press, Boca Raton, 1995).
[4]M. Winkler, X. Liu, A.-L. Hansen, J. D. König, W. Bensch, L. Kienle, H. Böttner, and K. Bartholomé, Nanothermoelectrics **1**, 1 (2013).
[5]R. Venkatasubramanian, T. Colpitts, E. Watko, M. Lamvik, and N. El-Masry, J. Cryst. Growth **170**, 817 (1997).
[6]R. Venkatasubramanian, E. Siivola, T. Colpitts, and B. O'Quinn, Nature **413**, 597 (2001).
[7]A.-L. Hansen, T. Dankwort, M. Winkler, J. Ditto, D. C. Johnson, J. D. Koenig, K. Bartholomé, L. Kienle, and W. Bensch, Chem. Mater. **26**, 6518 (2014).
[8]M. Winkler, X. Liu, U. Schürmann, J. D. König, L. Kienle, W. Bensch, and H. Böttner, Z. Anorg. Allg. Chem. **638**, 2441 (2012).
[9]For a recent review article see: T. Dankwort, A.-L. Hansen, M. Winkler, U. Schürmann, J. D. Koenig, D. C. Johnson, N. F. Hinsche, P. Zahn, I. Mertig, W. Bensch, and L. Kienle, Phys. Status Solidi A **213**, 662 (2016).
[10]M. Eschbach, E. Młyńczak, J. Kellner, J. Kampmeier, M. Lanius, E. Neumann, C. Weyrich, M. Gehlmann, P. Gospodarič, S. Döring, G. Mussler, N. Demarina, M. Luysberg, G. Bihlmayer, T. Schäpers, L. Plucinski, S. Blügel, M. Morgenstern, C. M. Schneider, and D. Grützmacher, Nat. Commun. **6**, 8816 (2015).
[11]Y. Jiang, Y. Y. Sun, M. Chen, Y. Wang, Z. Li, C. Song, K. He, L. Wang, X. Chen, Q.-K. Xue, X. Ma, and S. B. Zhang, Phys. Rev. Lett. **108**, 066809 (2012).
[12]X. Zhang, Z. Zeng, C. Shen, Z. Zhang, Z. Wang, C. Lin, and Z. Hu, J. Appl. Phys. **115**, 024307 (2014).
[13]Y. Saito *et al.*, Phys. Status Solidi B **252**, 2151 (2015).
[14]I. Hilmi, A. Lotnyk, J. W. Gerlach, P. Schumacher, and B. Rauschenbach, APL Mater. **5**, 050701 (2017).
[15]B. Saha, P. Chaturvedi, A. K. Yadav, D. Saha, and S. Ganguly, J. Vac. Sci. Technol. B **34**, 021806 (2016).
[16]G. Bendt, S. Zastrow, K. Nielsch, P. S. Mandal, J. Sánchez-Barriga, O. Rader, and S. Schulz, J. Mater. Chem. A **2**, 8215 (2014).
[17]P. I. Kuznetsov, B. S. Shchamkhalova, V. O. Yapaskurt, V. D. Shcherbakov, V. A. Luzanov, G. G. Yakushcheva, V. A. Jitov, and V. E. Size, J. Cryst. Growth **471**, 1 (2017).
[18]L. M. Conclaves, P. Alum, A. G. Rollo, and J. H. Corey, Thin Solid Films **519**, 4152 (2011).
[19]H. Shen, S. Lee, J.-G. Kang, T.-Y. Edom, H. Lee, and S. Han, Appl. Surf. Sci. **429**, 115 (2018).
[20]J.-H. Kim, J.-Y. Choi, J.-M. Bee, M.-Y. Kim, and T.-S. Oh, Mater. Trans. **54**, 618 (2013).
[21]J.-M. Lin, Y.-C. Chen, and W. Chen, J. Nanomater. **2015**, 564954.
[22]For a recent review article see: Y. Goo, Z. Liu, and H. Pang, Small **11**, 3290 (2015).
[23]H. Chi, W. Liu, and C. Usher, "Growth and transport properties of tetradymite thin films," in *Materials Aspect of Thermoelectricity*, 1st ed., edited by C. Uher (CRC Press, Boca Raton, 2016).
[24]P. Lošt'ák, Č. Drašar, A. Krejčová, L. Beneš, J. S. Dyck, W. Chen, and C. Uher, J. Cryst. Growth **222**, 565 (2001).
[25]P. Lošt'ák, Č. Drašar, J. Horàk, Z. Zhou, J. S. Dyck, and C. Uher, J. Phys. Chem. Solids **67**, 1457 (2006).
[26]J. M. Yáñez-Limón, J. González-Hernández, J. J. Alvaro-Gil, I. Delgadillo, and H. Vargas, Phys. Rev. B **52**, 16 321 (1995).
[27]C. E. Raudzis, Ph.D. thesis, Der andere Verlag, 2007.
[28]D. G. Cahill, Rev. Sci. Instrum. **61**, 802 (1990).
[29]T. Borca-Tasciuc, A. R. Kumar, and G. Chen, Rev. Sc. Instrum. **72**, 2139 (2001).
[30]T. Tong and A. Majumdar, Rev. Sci. Instrum. **77**, 104902 (2006).
[31]P. Dutta, D. Bhoi, A. Midya, N. Khan, P. Mandal, S. S. Samatham, and V. Ganesan, Appl. Phys. Lett. **100**, 251912 (2012).
[32]M. de Jong, W. Chen, T. Angsten, A. Jain, R. Notestine, A. Gamst, M. Sluiter, C. K. Ande, S. van der Zwaag, J. J. Plata, C. Toher, S. Curtarolo, G. Ceder, K. A. Persson, and M. Asta, Sci. Data **2**, 150009 (2015).
[33]D. Zheng, S. Tanaka, K. Miyazaki, and M. Takashiri, J. Electron. Mater. **44**, 1679 (2015).
[34]Z. Wei, J. Yang, W. Chen, K. Bi, D. Li, and Y. Chen, Appl. Phys. Lett. **104**, 081903 (2014).
[35]Q. Fu, J. Yang, Y. Chen, D. Li, and D. Xu, Appl. Phys. Lett. **106**, 031905 (2015).
[36]H. Zhang, X. Chen, Y.-D. Jho, and A. J. Minnich, Nano Lett. **16**, 1643–1649 (2016).
[37]B.-T. Wang, P. Souvatzis, O. Eriksson, and P. Zhang, J. Chem. Phys. **142**, 174702 (2015).
[38]J. Horák, K. Čermák, and L. Koudelka, J. Phys. Chem. Solids **47**, 805 (1986).
[39]Y. S. Ju and K. E. Goodson, Appl. Phys. Lett. **74**, 3005 (1999).
[40]Q. Zhang, C. Liu, X. Liu, J. Liu, Z. Cui, Y. Zhang, L. Yang, Y. Zhao, T. T. Xu, Y. Chen, J. Wei, Z. Mao, and D. Li, ACS Nano **12**, 2634 (2018).
[41]H.-K. Lyeo and D. G. Cahill, Phys. Rev. B **73**, 144301 (2006).
[42]A. S. Pashinkin, A. S. Malkova, and M. S. Mikhailova, Russ. J. Phys. Chem. **82**, 878 (2008).
[43]C. Chiritescu, D. G. Cahill, N. Nguyen, D. Johnson, A. Bodapati, P. Keblinski, and P. Zschack, Science **315**, 351 (2007).
[44]L. Wu, Q. Meng, C. Jooss, J.-C. Zheng, H. Inada, D. Su, Q. Li, and Y. Zhu, Adv. Funct. Mater. **23**, 5728 (2013).

DOI: 10.1063/1.5025491
URN: urn:nbn:de:hbz:464-20201214-174153-8